Solid State Phenomena
ISSN: 1662-9779, Vol. 387, pp 61-73
doi:10.4028/p-Wf7rKC

Submitted: 2026-01-14
Revised: 2026-02-16
Accepted: 2026-02-17
Online: 2026-04-14

Thermo-Chemical Modeling and Experimental Validation of Pultruded Glass Fiber Reinforced Composites

Jacob Harris[1,a*], Sangharsha Gharat[1,b], Luohaoran Wang[1,c], Ali Zolali[2,d], Alan Taub[1,e] and Mihaela Banu[1,f]

[1]University of Michigan, Ann Arbor, USA

[2]BASF, Wyandotte, USA

[a]jchari@umich.edu, [b]sgharat@umich.edu, [c]lhrwang@umich.edu, [d]ali.zolali@basf.com, [e]alantaub@umich.edu, [f]mbanu@umich.edu

Keywords: pultrusion, thermo-chemical modeling, cure kinetics, glass fiber composites.

Abstract. This work develops and validates thermo-chemical models for pultrusion of glass fiber–reinforced polyurethane composites on an industrial PulFlex production line. A reduced one-dimensional model combining a calibrated Kamal–Sourour (KS) cure law with an Arrhenius type chemo-rheological viscosity formulation is cross-validated against a three-dimensional ANSYS Composite Cure Simulation using identical material inputs along a three-zone, 0.9144 m heated die. Embedded thermocouples provide in-die temperature histories at 50.8 cm·min^{-1} for calibration, while additional differential scanning calorimetry (DSC) measurements supply degree of cure (DoC) profiles for independent validation. At the industrial operating speed of 50.8 cm·min^{-1}, the mathematical and ANSYS models both reproduce the measured temperature peak location and exit temperature within a few degrees Celsius and predict a die-exit DoC of approximately 0.95, confirming near-complete curing. Using these calibrated fields as inputs to an analytical pulling-resistance formulation, both models predict comparable pulling force magnitudes and plateau behavior, demonstrating that the simplified 1D framework can capture not only thermo-chemical evolution but also process resistance trends over a range of pulling speeds. The validated 1D model therefore enables efficient exploration of speed–temperature–force tradeoffs for process window design, while the 3D ANSYS model provides a higher-fidelity reference for local gradients and future thermo–chemo–mechanical extensions.

1. Introduction

The manufacturing of continuous fiber-reinforced polymer composites through pultrusion is widely valued for its ability to streamline production through a highly automated and continuous process [1,2]. Because the material is shaped as it is pulled through the die, long, straight components can be produced in a single pass without additional joining operations, reducing manufacturing time, cost, and material waste [1,2–5]. These advantages have driven the adoption of pultruded composites across automotive, aerospace, construction, and renewable energy applications [4,5].

Despite its industrial maturity, pultrusion is inherently complex due to strong coupling among heat transfer, resin flow, chemical cure reactions, pressure evolution, and stress development, all of which influence process stability, final part quality, and dimensional accuracy [1,2,4–6]. The process involves multiple critical stages including fiber alignment, resin impregnation, heating, curing, and controlled pulling speed, with thermal management playing a central role in gelation and cure completion [1–7].

Physics-based computational modeling has therefore become an essential complement to empirical process development in pultrusion [6,8,9]. Coupling finite-element heat transfer with cure kinetics enables prediction of temperature evolution and DoC progression along the die, providing early insight into process behavior prior to physical trials [6–10]. For example, Liu et al. demonstrated that increasing pulling speed delays the exothermic peak and reduces in-die cure due to shortened residence time [10]. Similar modeling frameworks have been validated under a range of processing

conditions and extended to impregnation modeling in closed injection pultrusion, where flow through porous fiber beds becomes dominant [11].

To ensure reliability under industrial conditions, such models must be validated against representative process measurements. In this study, we develop and experimentally validate thermo-chemical pultrusion models for glass fiber–reinforced polyurethane composites processed on an industrial pultrusion line at PulFlex, Pittsburgh, PA. Embedded thermocouples in the die's provide transient temperature histories for model calibration and validation. In addition, a reduced one-dimensional mathematical model is cross-compared against a detailed three-dimensional ANSYS Composite Cure Simulation using identical cure kinetics and chemo-rheological inputs. This direct comparison isolates the influence of modeling dimensionality and heat-transfer assumptions, providing a quantitative basis for assessing the applicability of the reduced model for parametric studies while retaining ANSYS as a higher-fidelity reference for local effects.

2. Methodology

2.1. Process configuration and operating conditions

Pultrusion experiments were conducted on the PulFlex Technologies industrial line, consisting of a closed resin-impregnation/injection stage, a heated forming/cure die, and dual-belt pullers (Fig. 1(a-c)). Continuous fiber rovings were guided from creels through alignment cards into the closed injection box. A two-component polyurethane (PU) resin system was supplied by a metering/mixing unit that combined the polyol component (Elastocoat 74850R) and isocyanate component (Elastocoat 74850T) at a target stoichiometric ratio of 1.17:1 (isocyanate: polyol).

Fig. 1. Schematic of the PulFlex line pultrusion process: (a) resin impregnation via MVP injection box, (b) three-zone heated forming die, (c) in-line puller.

Immediately downstream of the injection region, the saturated fiber bundle entered a three-zone steel forming die (Fig. 1(b)) that produced a constant rectangular profile of 127 mm × 3.2 mm (Fig. 2). The die contained three independently controlled electric heating zones set to 133 °C, 177 °C, and 154 °C (Zones 1–3), with a combined heated length of approximately 0.914 m. The pulling speed was varied between 48.3 and 63.5 cm·min^{-1}. An operating condition of 50.8 cm·min^{-1} provided stable production with consistent part quality and was selected as the reference condition for model calibration and ANSYS–mathematical model comparison. Post-cure measurements confirmed the part cross-section was consistent with the die design (Fig. 2).

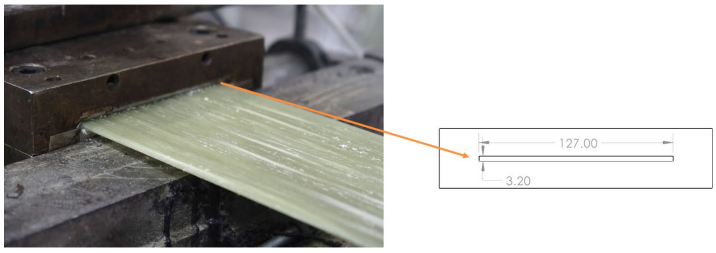

Fig. 2. Pultruded part at die exit (left: optical image) and measured cross-sectional dimensions (right: cross section of the die: 127 mm width × 3.2 mm thickness).

2.2 Experimental trials, data acquisition and instrumentation

To capture the in-die thermal history, a K-type thermocouple was embedded directly within the reinforcement bundle by tying it to a central tow upstream of the injection box. The sensor provided a continuous temperature record as a function of time and position along the die (Fig. 3(a)). The temperature–position measurement at the pulling speed of 50.8 cm·min^{-1} (Fig. 3(b)) was used as the primary dataset for thermo-chemical model calibration. Die-wall thermocouples in each heating zone monitored die surface temperature and verified that programmed setpoints were maintained during each trial.

To validate the curing behavior extracted from simulation, a Differential Scanning Calorimetry (DSC) methodology by TA Discovery DSC 2500 employed a specific thermal profile designed to characterize the resin's curing kinetics under conditions that simulate the rapid heating of the real pultrusion process by PulFlex, Pittsburgh, PA. The material was subjected to a multi-step temperature program characterized by aggressive ramp rates of 200.00 °C/min starting from 50 °C, reaching setpoints of 133.00 °C, 177.00 °C, and 156.00 °C, interspersed with short 0.3-minute isothermal holds. This rapid thermal cycling mimicked the environment within the die where the resin transitions from a liquid to a rubbery status (gelation), eventually leading to the final cure. The final stages of the test involved cooling down to 25.00 °C followed by a standard ramp to 200.00 °C, likely to assess the residual cure of the processed PU.

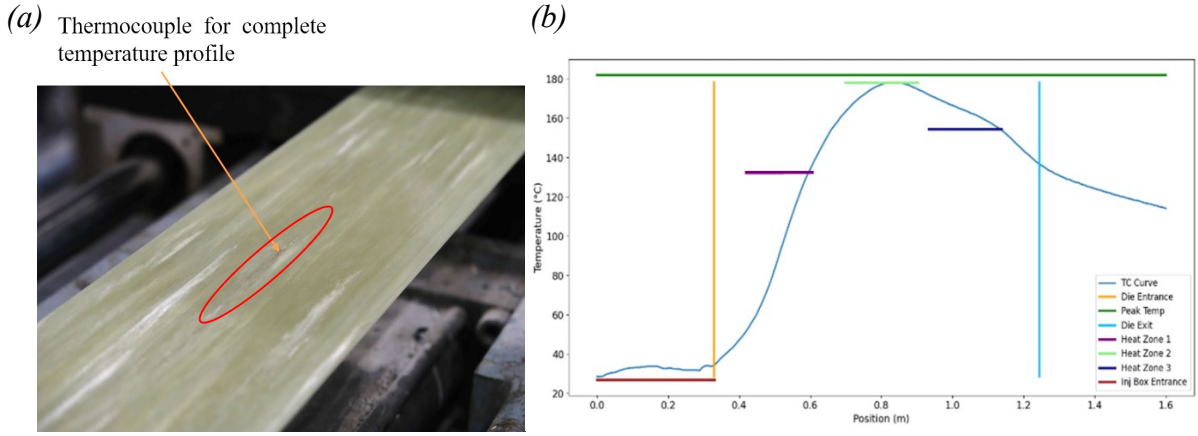

Fig. 3. Thermocouple-based temperature acquisition: (a) sensor placement in composite preform, (b) temperature profile along die length at 50.8 cm·min^{-1}.

In this work, the thermo-chemical model focuses on three coupled physical phenomena which are axial heat transfer along the die, resin cure kinetics, and the resulting evolution of viscosity. These physical processes were chosen as they directly control the temperature history, gelation position, degree of cure, and pulling resistance in thermoset pultrusion [3]. Other mechanisms such as compaction in a tapered entrance and detailed resin flow in the injection region was not modeled explicitly, since the PulFlex configuration employs a constant-section die without a compaction taper and the trials showed stable impregnation in the glass-fiber baseline trials. Prior studies indicate that viscous drag and friction dominate the pull force while compaction and local flow variations make a comparatively minor contribution [12].

3. Finite Element Modeling of Thermal and Curing Phenomena in Pultrusion Manufacturing

3.1 Geometric configuration, mesh generation and boundary conditions

The composite laminate was modeled in ANSYS Composite PrepPost (ACP) to capture through-thickness thermal gradients and anisotropy. The laminate consisted of 0.2 mm plies (total thickness 3.2 mm) with a width of 127 mm, matching the experimental profile.

The three-dimensional finite element simulation was implemented to capture the full thermal-chemical coupling during the pultrusion process. The composite laminate was meshed using 8-node

brick elements (SOLID278 in ANSYS) with body sizing and a smallest feature size of 0.2 mm. Additionally, side biasing was applied at corners to capture high gradient regions, resulting in approximately 2.1 million elements for the full composite length. The die structure was meshed with a smallest feature size of 3 mm using a 4-biased boundary-constrained mesh scheme. For the internal surface of the die, face meshing was applied with a minimum element size of 0.3 mm to ensure accurate resolution of the die-composite interface thermal interactions. These meshing strategies enabled precise representation of heat transfer at critical interfaces.

To complete the thermal model formulation, boundary conditions were applied to represent the physical heat transfer mechanisms. Contact between the die and composite surfaces was defined using surface-to-surface contact pairs, with the die internal surface as the target and the composite outer surface as the contact. A coefficient of convective heat transfer of 5000.0 W/(m²·°C) was applied at this interface, with a friction coefficient of 0.25 to capture resistance during pulling. Natural convection with a heat transfer coefficient of 10 W/m²·K at 25 °C ambient was applied to external die surfaces. These thermal boundary conditions, coupled with the material properties and cure kinetics, establish the complete computational framework for process simulation.

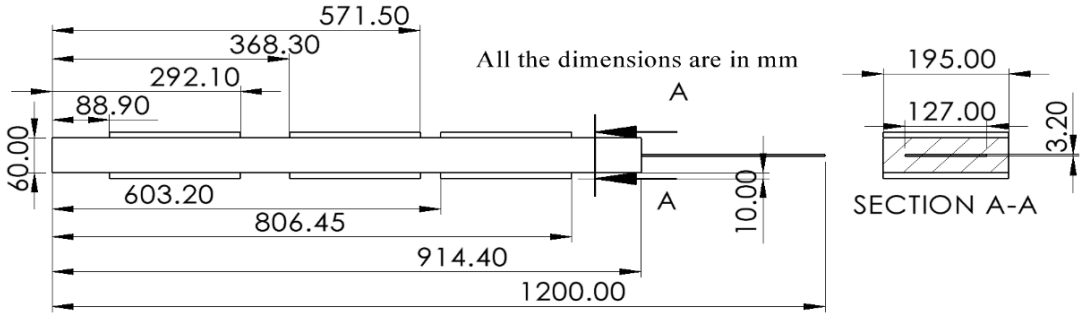

Fig. 4. Longitudinal die-composite system geometry and actual dimensions of the PulFlex pultruder, and the cross section (Section A-A) of the last segment of the die which define the final pultruded geometry.

The dimensions presented in Fig. 4 were used for creating the pultrusion finite element simulation displayed in the following paragraph.

3.2 Computational framework

The study of thermo-chemical evolution and polymerization kinetics in pultrusion required developing a computational model of both the die and fiber-reinforced polymer matrix. This approach enabled quantification of heat transfer mechanisms and thermo-mechanical effects under industrial conditions. Simulations used ANSYS 2025 R1 with the ANSYS Composite Cure Simulation (ACCS) module for polymerization, thermal fields, and multiphysics coupling in thermoset composites. The transient energy conservation equation for the curing composite incorporated diffusive and advective transport with volumetric heat from exothermic reactions, as presented in Eq. 1:

$$\rho c_p \left(\left(\frac{\partial T}{\partial t} \right) + u \left(\frac{\partial T}{\partial x_c} \right) \right) = - \left(\left(\frac{\partial}{\partial xo} \right) Qo \right) + H_i \, . \tag{1}$$

where ρ is the density of material, c_p is the specific heat of the composite material, T is the temperature, Q_o is the heat flux, H_i characterizes the rate of internal heat generation per unit volume due to curing reactions, and the convective term $u \left(\frac{\partial T}{\partial x_c} \right)$ accounts for thermal advection resulting from material transport through the die at the prescribed pulling velocity.

For the metallic die structure, thermal transport was governed by classical Fourier conduction with material advection in the primary pulling direction, as presented in Eq. 2:

$$\rho c_p \left(u \frac{\partial T}{\partial x} \right) = K_x \frac{\partial^2 T}{\partial x^2} + K_y \frac{\partial^2 T}{\partial y^2} + K_z \frac{\partial^2 T}{\partial z^2} + q. \tag{2}$$

where ρ is the density of matrix, c_p is the specific heat, K_x, K_y, K_z represent the directional thermal conductivities along the longitudinal (x), and transverse (y, z) axes, while q denotes internally generated heat. The pulling velocity u in the longitudinal direction introduces a Eulerian advection term that reflects the continuous material flow through the stationary die assembly.

Equivalent pressure stress p is a scalar measure of the hydrostatic component of the stress tensor, as presented in Eq. 3:

$$p = -\frac{1}{3} \times (\sigma_{11} + \sigma_{22} + \sigma_{33}) \quad (3)$$

where σ_{11} is normal stress in the pultrusion direction, σ_{22} is normal stress in the transverse direction, and σ_{33} is normal stress in the thickness direction.

The total pulling force required during the pultrusion process was determined as the sum of three force components [12], as presented in Eq. 4:

$$F_{d,total} = F_{com} + F_{vis} + F_{fric} \quad (4)$$

where F_{com} is the compaction force, F_{vis} is the viscous drag force, and F_{fric} is the friction force. The compaction force, given by equation (5), was zero in this study as no tapered die inlet was employed ($\theta = 0°$):

$$F_{com} = \int_{x=0}^{x=L_t} 2w(\dot{p} + \sigma) tan\theta \, dx \quad (5)$$

The viscous force was calculated using equation (6) by integrating the shear stress over the pre-gelation region from the die entrance to position x_{in}:

$$F_{vis} = \int_{x=0}^{x=x_{in}} 2w\tau \, dx \quad (6)$$

where w is the composite width (0.127 m) and τ is the shear stress calculated using the viscosity at different pulling speeds and thickness. The friction force acting in the post-gelation region was determined as by equation (7):

$$F_{fric} = \int_{x=x_{in}}^{x=x_L} 2wf\sigma \, dx \quad (7)$$

where f is the coefficient of friction (0.3) [13], and x_L is the die exit position (0.9144 m). Material shrinkage effects were not considered in this analysis.

3.3 Cure evolution and flow behavior modeling

Curing of the PU was characterized through DSC measurements leading to the following set of values (Table 1), where E_a is the activation energy for curing, H_{tot} is the total heat released, A_1 and A_2 are the pre-exponential factors and m is the autocatalytic reaction order and n is the reaction order for remaining reactants.

Table 1. Curing Kinetics of PU Derived from DSC Measurements.

Parameters	Values	Units
Activation energy (E_a)	46.12	[kJ/mol]
Total heat released (H_{tot})	127.17	[kJ/kg]
A_1	1.0×10^{-2}	[1/s]
A_2	3.52×10^{4}	[1/s]
m	0.11	-
n	1.64	-

In the same time, the cure evolution was modeled using the KS autocatalytic kinetic law, as presented in Eq. 8:

$$\frac{d\alpha}{dt} = (E_1 + E_2\,\alpha^m)(1-\alpha)^n. \quad (8)$$

Here, α is DoC (0 to 1), and $E_1, E_2, m,$ and n define the reaction rate and autocatalytic behavior. Resin viscosity was modeled as a coupled function of temperature T and the degree of crystallinity (DoC), denoted α, as presented in Eq. 9:

$$\eta(T,\alpha) = \eta_\infty \exp\left(\frac{U}{RT} + K_\eta \alpha\right). \quad (9)$$

In Eq. (9), η_∞, U, and K_η are empirical constants and R is the universal gas constant. The viscosity and cure inputs were coupled through the thermal–cure solution governed by Eqs. (1-2, 8-9).

3.4. Integration of Viscosity for Pulling Force Prediction

To predict the pulling force requirements as a function of pulling speed, a coupled thermo-chemo-mechanical framework was implemented. A displacement-controlled boundary condition was applied at the composite inlet, where the displacement magnitude at each time step corresponded to the specified pulling velocity (displacement = velocity × Δt, with Δt = 1 second). This approach simulated the continuous material flow through the die under quasi-steady-state conditions.

The viscosity field, obtained from the chemo-rheological model as a function of local temperature and degree of cure, was computed at every integration point throughout the simulation. This viscosity distribution served as the constitutive input for calculating shear stresses in the pre-gelation region. Simultaneously, the simulation calculated normal stress components ($\sigma_{11}, \sigma_{22}, \sigma_{33}$) at each position, which were extracted to determine the pressure distribution acting on the composite-die interface. The gelation position was identified, separating the viscous-dominated pre-gelation zone from the friction-dominated post-gelation zone.

The total pulling force was determined by integrating the viscosity-dependent shear stress over the pre-gelation region and adding the friction force contribution from the post-gelation region, calculated using the extracted normal stresses and a constant friction coefficient (μ = 0.3). Material shrinkage effects were not considered in this analysis. The constant friction coefficient results in constant friction force post-gelation, causing the total pulling resistance to plateau after gelation.

3.5. Computational results and process parameter analysis

The transient simulation employed a time step of 1 second with the three heating zones set to 133°C (Zone 1), 177°C (Zone 2), and 154°C (Zone 3). As the composite progresses through the die, the polymer undergoes distinct phase transformations: in Zone 1(starting at x = 88.9 mm), the material remains in a low-viscosity liquid state as temperature rises; upon entering Zone 2 (starting at x = 368.3 mm), the elevated temperature triggers rapid polymerization and the material transitions through gelation into a rubber-like state; by the end of Zone 2 (ending at x = 571.5 mm) and through Zone 3 (ending at x = 806.45 mm), the material approaches vitrification, transforming into a rigid, fully consolidated solid. The simulated temperature distribution at a pulling speed of 50.8 cm·min^{-1} is shown in Fig. 5, with a peak temperature of approximately 174 °C in the mid-die region after complete simulation.

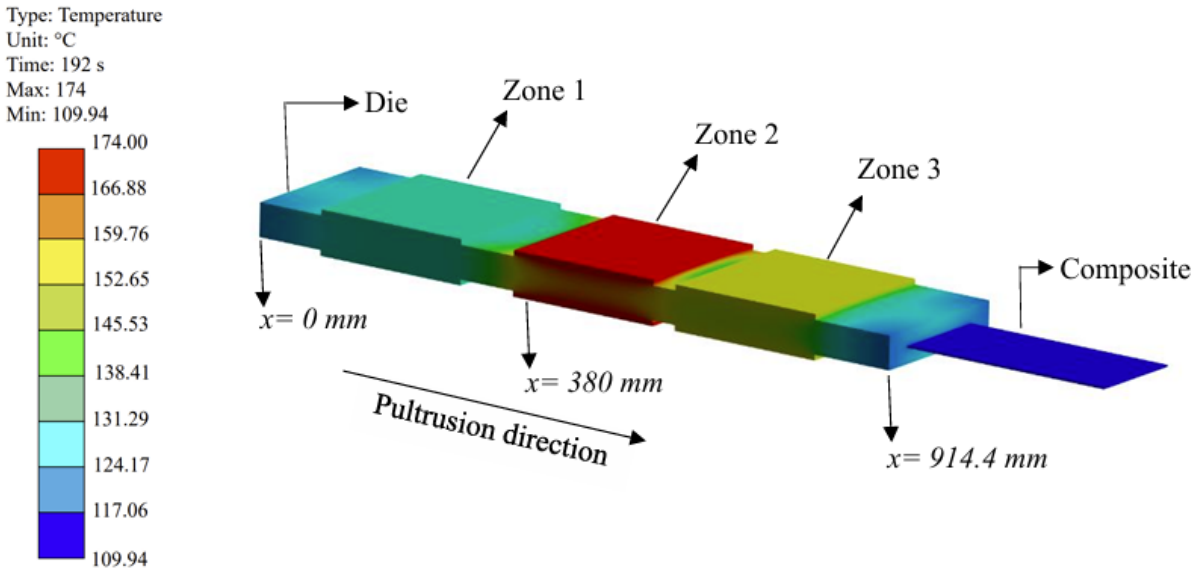

Fig. 5. Temperature contours along the die and composite in ANSYS 2025 R1.

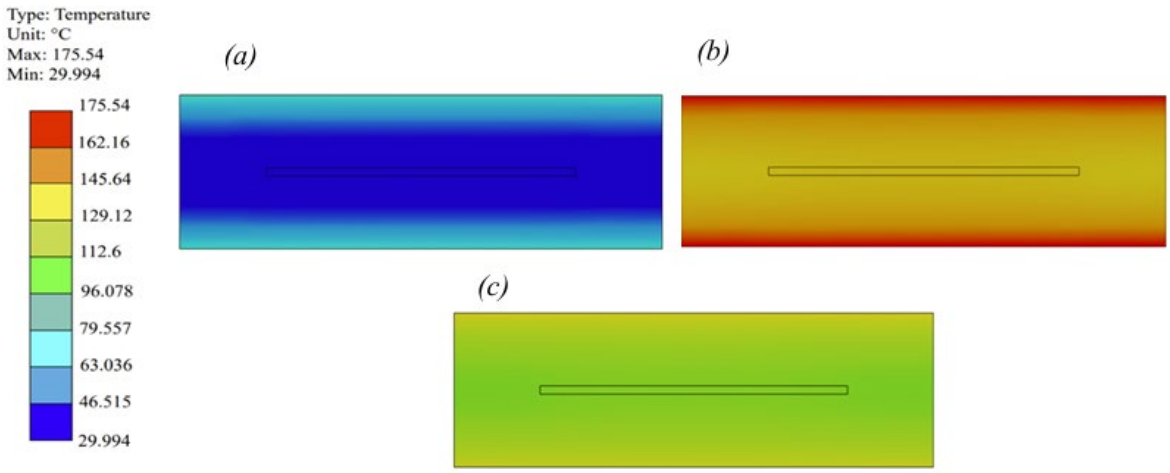

Fig. 6. Cross-sectional temperature contour distributions at three axial locations: (a) length x = 0 mm, (b) length x = 380 mm, (c) length x = 914.4 mm.

Three cross-sections are also shown in Fig. 6, at: (a) x = 0 mm at the die entrance, (b) x = 380 mm after the start of zone 2 heating at 177 °C, and (c) x = 914.4 mm at the die exit. To quantify process sensitivity, the validated ACCS model was evaluated across a range of pulling speeds, and Fig. 7 summarizes the coupled evolution of (a) temperature, (b) DoC, (c) pulling force, and (d) die-exit conversion versus speed along the 0.9144 m die length.

The temperature profiles along the die for different pull speeds are shown in Fig. 7(a). In all cases, the temperature increases from the inlet, reaches a peak of about 170–180 °C in the mid-die region (around 0.45–0.6 m) due to die heating and reaction exotherm, and then decreases toward the die exit. Fig. 7(b) presents the degree of cure (DoC) evolution along the die. Although the cure develops progressively along the heated zone, the key difference is observed at the die exit, where the DoC decreases with increasing pull speed. Lower pull speeds achieve faster cure development and near-complete conversion earlier in the die, whereas higher speeds shift the cure onset downstream and result in lower conversion at the exit, highlighting the strong influence of residence time on cure kinetics.

Figure 7(c) shows the evolution of pulling force along the die length for different pulling speeds ranging from 10 to 90 cm·min^{-1}. At lower pulling speeds (10–20 cm·min^{-1}), the force rise occurs

earlier in the die and reaches plateau values of approximately 6500–7000 N, while higher speeds (48.3–90 cm·min⁻¹) shift the force increase downstream and result in higher plateau forces (7000–8500 N). This trend reflects the delayed gelation at faster speeds due to reduced residence time, which increases the pre-gelation viscous contribution before the transition to friction-dominated pulling. The sharp increase in all curves confirms the transition of the gelation, while the constant post-gelation force validates the assumption of constant friction coefficient in the cured composite region.

In Fig. 7(d) the DoC at die exit as a function of pull speed decreases monotonically from about 99.52% at 10 cm·min⁻¹ to 88.38% at 90 cm·min⁻¹. This trend demonstrates the tradeoff between productivity and cure completeness, indicating that pull speeds above ~50 cm·min⁻¹ may lead to under-cured profiles for the present die and resin system unless compensated by modified thermal conditions or post-curing.

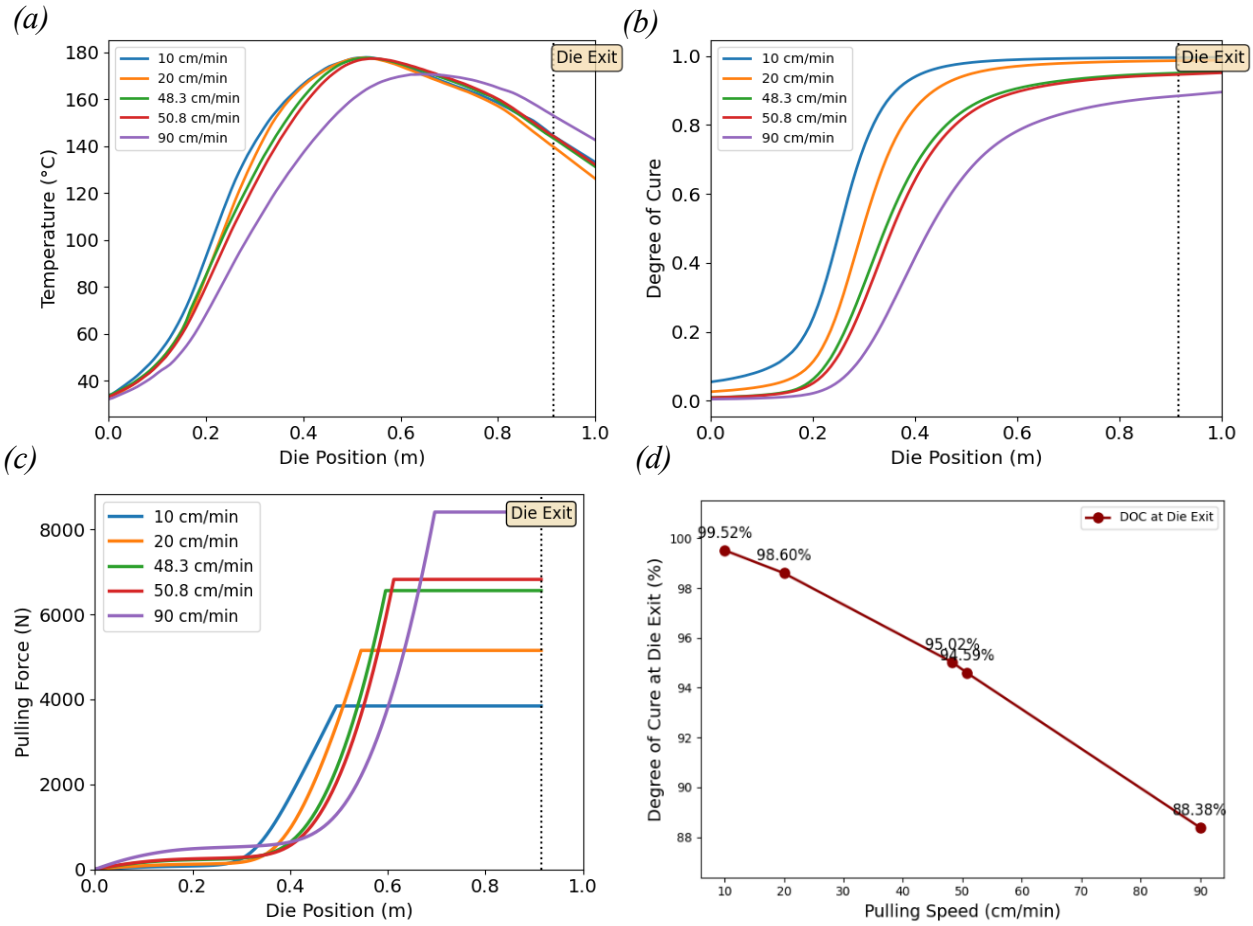

Fig. 7. Coupled (a) temperature, (b) DoC, (c) pulling force, and (d) cure at die exit for pulling speeds ranging from 10-90 cm·min⁻¹.

4. Mathematical Modeling of Thermal and Curing Phenomena in Pultrusion Manufacturing

4.1. Modeling framework and parameter identification

A reduced-order thermo-chemical model was developed to reproduce the PulFlex glass fiber pultrusion trials and enable rapid, speed-dependent predictions of temperature, DoC, and viscosity along the heated die. Glass fibers (ECT469PH CPIC Abahsain Fiberglass) were used for calibration due to their stable thermocouple measurements. The heated die length was set to 0.9144 m and divided into three heater zones. Zone setpoints were represented as piecewise-constant heater bands superimposed on a smooth baseline centerline temperature profile $T(x)$ (Fig. 8). The baseline $T(x)$ was calibrated using the 50.8 cm·min⁻¹ thermocouple trace and exhibits a single peak near $x \approx 0.47m$ followed by cooling toward the die exit, consistent with prior pultrusion modeling studies [14].

Predictions at other pulling speeds v were obtained by applying speed-dependent scaling to the peak temperature, exit temperature, and rise/decay exponents of $T(x)$, while preserving the experimentally observed peak location and accounting for reduced residence time at higher speeds. The local DoC $\alpha(x)$ was computed by integrating the KS autocatalytic kinetic model defined in Eq. (8), using the local thermal history provided by $T(x)$. Kinetic parameters were identified from DSC measurements following established procedures [15,16] and are summarized in Table 1.

The governing cure equation was integrated into a Lagrangian frame with $\Delta t = \Delta x/v$, using a two-stage explicit time-integration scheme with midpoint temperature evaluation. Resin viscosity was computed using the Arrhenius-type chemo-rheological relationship given in Eq. (9), consistent with the formulation used in the ANSYS Composite Cure Simulation module. In Eq. (9), η_∞, U, and K denote the reference viscosity, apparent activation energy for flow, and cure-dependent stiffening parameter, respectively. These viscosity parameters were calibrated such that the predicted centerline viscosity at 50.8 cm·min^{-1} matched the ANSYS results and were subsequently held fixed across all pulling speeds. Following common practice for reactive thermosets, gelation was defined as the axial location where $\eta \geq 10^4$Pa·s [16,17], with residence time given by $t(x) = x/v$. The composite was treated as a one-dimensional unidirectional laminate with a fiber volume fraction of $V_f = 0.60$.

4.2 Results and discussion of the mathematical model

Fig. 8 presents the predicted centerline temperature distributions along the 0.9144 m heated die for pulling speeds of 5.0, 20.0, 48.3, 50.8, and 90.0 cm·min^{-1}. In all cases, temperature increases rapidly from the die entrance to approximately 0.45–0.50 m, followed by a gradual decrease toward the exit. At lower pulling speeds (5–20 cm·min^{-1}), the longer residence time allows the composite to approach the heater-zone setpoint temperatures farther upstream in the die. As pulling speed increases, reduced residence time lowers both peak and exit temperatures. These trends are consistent with classical pultrusion heat transfer behavior, in which increasing speed shifts thermal features downstream and limits internal temperature rise [14].

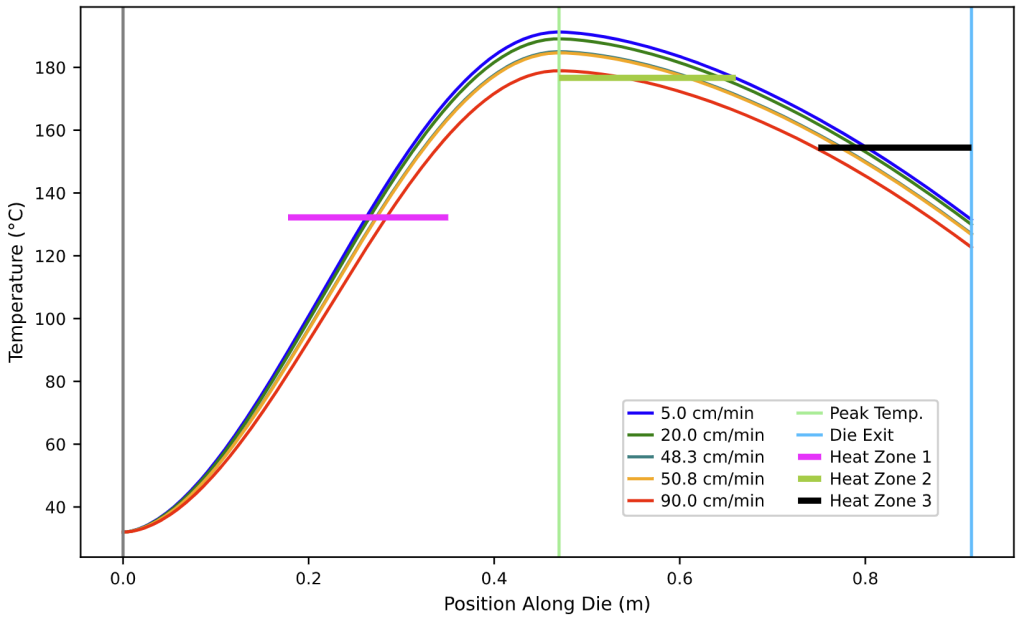

Fig. 8. Mathematical modeling of composite temperature profile along heating die.

The corresponding DoC evolution is shown in Fig. 9(a). For all pulling speeds, the cure profiles exhibit the characteristic Kamal–Sourour S-shaped behavior. Increasing pulling speed shifts the main cure rise downstream and reduces die exit DoC due to shortened residence time. At the reference speed of 50.8 cm·min^{-1}, the model predicts a die-exit DoC of approximately 0.95, consistent with experimental observations of near-complete curing under this condition.

The predicted pulling force evolution along the 0.9144 m die is presented in Fig. 9(b). For each pulling speed, the total force increases from near zero at the inlet to a plateau in the post-gelation

region as the contribution from viscous drag is replaced by friction at the die–composite interface. At lower speeds (10–20 cm·min^{-1}), the force rise occurs earlier in the die and plateaus at moderate levels, reflecting earlier gelation and shorter viscous-dominated length. At higher speeds (48.3–90 cm·min^{-1}), the force increase is shifted downstream, and the plateau magnitude becomes larger, indicating a longer pre-gelation shear zone and greater integrated resistance before friction dominates. The sharp change in slope around the gel point in all curves confirms the transition between viscous-dominated and friction dominated pulling resistance assumed in the analytical formulation.

The dependence of die-exit DoC on pulling speed is summarized in Fig. 9(c). The model predicts a monotonic decrease in exit DoC with increasing speed. Using a practical in-die DoC target of 95%, the current heater schedule supports pulling speeds up to approximately 50–55 cm·min^{-1} without significant cure deficit. Speeds well below 20 cm·min^{-1} provide only marginal gains in exit DoC while reducing throughput, whereas higher speeds push the primary gelation transition too close to, or beyond, the die exit. The predicted temperature, cure, and viscosity fields at 50.8 cm·min^{-1} are subsequently used as baseline inputs for comparison with the full ANSYS thermo-chemical simulation in Section 5.

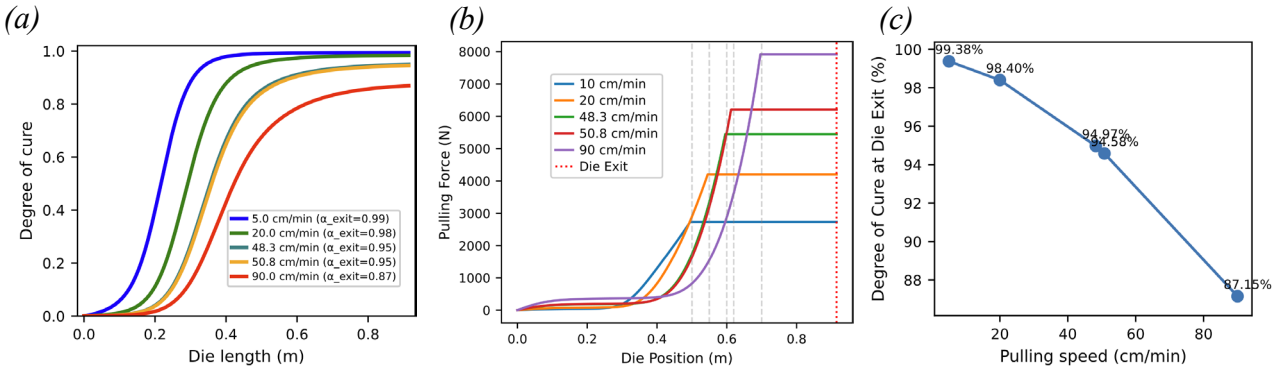

Fig. 9. Mathematical modeling of (a) DoC, (b) Pulling force, and (c) DoC at die exit.

5. Comparison of ANSYS Simulation and Mathematical Modeling in Pultrusion Manufacturing

To evaluate the reliability of the reduced mathematical model and its suitability for process design, its predictions were compared directly with both experimental measurements and the full thermo-chemical ANSYS simulation at a pulling speed of 50.8 cm·min^{-1}. All three modeling approaches employed identical experimentally calibrated cure kinetics, while the ANSYS and mathematical models shared the same chemo-rheological viscosity formulation used for pulling-force prediction.

Figure 10(a) compares the predicted and measured centerline temperature evolution along the heated die. The PulFlex thermocouple trace exhibits rapid heating from the inlet, a single peak in the mid-die region, and cooling toward the exit. Both the ANSYS and mathematical models reproduce this overall shape, capturing the peak location and exit temperature within a small offset that likely reflects local heat-transfer non-uniformities and sensor placement uncertainty. The DSC based temperature representation, constructed from the programmed oven history used in the cure kinetics experiments, shows a slightly sharper thermal ramp but follows the same peak range, reinforcing consistency between the laboratory characterization protocol and the industrial die conditions.

Figure 10(b) presents a comparison of DoC along the die between the mathematical model, the ANSYS Composite Cure Simulation, and the DSC-derived degree of cure at 50.8 cm·min^{-1}. The mathematical and ANSYS predictions exhibit closely aligned S-shaped cure profiles, with similar onset, inflection position, and die-exit DoC values (~0.95), consistent with near-complete curing inferred from post-process characterization. The DSC based DoC curve, when mapped to the die length using the measured temperature history, falls between the two model predictions and confirms that both frameworks reproduce the effective cure progression under the industrial heating schedule. Small offsets near the peak reaction zone are attributed to differences in heating rate between the pultruder and DSC protocol as well as through-thickness averaging in the 3D simulation

Figure 10(c) compares the pulling-force evolution along the die for the ANSYS based and mathematical models at 50.8 cm·min⁻¹. Despite their different dimensionality and numerical implementation, both models predict a similar structure: a gradual force increase in the upstream, low-viscosity region, a sharper rise around the gelation point, and an approximately constant plateau in the post-gelation segment where friction dominates. The predicted plateau levels differ by a modest margin that is within the combined uncertainty associated with friction coefficient, pressure distribution, and die–composite contact assumptions. Overall, the agreement in temperature, DoC, and pulling force indicates that the reduced 1D model is sufficient to reproduce key thermo-chemical and process-resistance features at the baseline operating condition, making it a practical tool for parametric studies while retaining the 3D ANSYS model as a benchmark for localized effects such as through-thickness gradients and die corner regions.

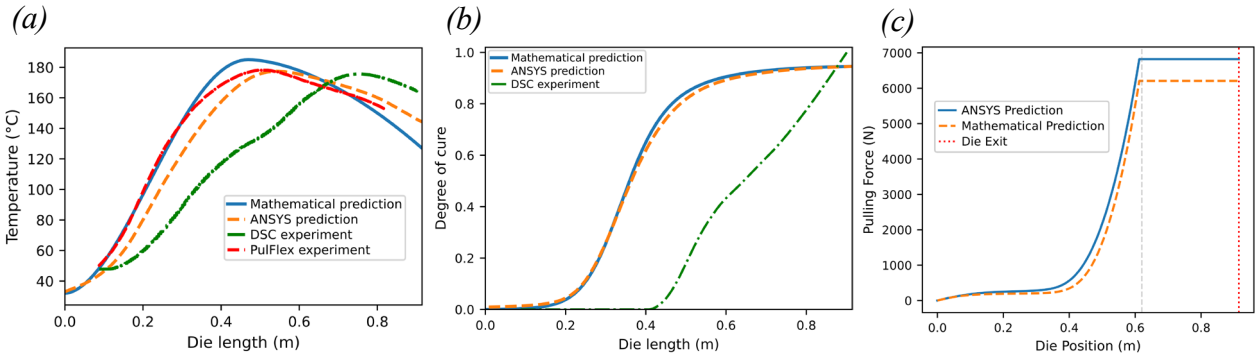

Fig. 10. Experimental and modeling prediction comparison at a 50.8 cm·min⁻¹ pulling speed for composite (a) Temperature, (b) DoC, and (c) Pulling force.

The current thermo–chemo framework predicts temperature, DoC, and pulling force along the PulFlex line but does not yet capture the mechanical response of the profile. Future work will extend the model to a coupled thermo–chemo–mechanical formulation that tracks modulus, stress, and strain evolution through the heated die, enabling prediction of residual stresses and cracking in complex profiles [18]. This extension will allow direct links between heater setpoints, pulling speed, and resulting mechanical performance.

In parallel, in-situ ultrasonic monitoring will be integrated to detect internal defects such as porosity and delamination during processing. Prior studies demonstrate the effectiveness of ultrasonic through-thickness, guided waves, and phased array techniques for defect detection in composite manufacturing [19,20]. These measurements will be combined with simulation outputs to predict defect localization and process optimization. Data assisted correction strategies can also be implemented to improve accuracy under industrial noise [21,22]. Finally, the framework will be extended to additional fiber and resin systems by updating kinetic, rheological, and modulus parameters to explore processing windows for various composite architectures [18].

Conclusion

This work developed and experimentally validated a thermo-chemical modeling framework for polyurethane-based pultrusion on an industrial PulFlex line using a glass fiber baseline. A reduced one-dimensional mathematical model combining a calibrated KS cure law with an Arrhenius-type chemo-rheological viscosity formulation was implemented to predict temperature, degree of cure, and pulling resistance along a three-zone, 0.9144 m heated die. In parallel, a three-dimensional ANSYS Composite Cure Simulation of the die–composite system was constructed using identical kinetic and rheological inputs, enabling direct comparison between reduced and finite element approaches.

Both models capture the dominant thermo-chemical behavior of the process and reproduce measured in-die temperature profiles at 50.8 cm·min⁻¹ within a few percent. The predicted DoC fields from ANSYS and the mathematical model agree closely with each other and with DSC-based reconstructions, yielding a die-exit DoC of approximately 0.95 and confirming near-complete curing

at the industrially preferred pulling speed. When these fields are used as inputs to an analytical pulling-force formulation, the ANSYS and reduced models predict similar force rise and plateau behavior along the die, demonstrating that the simplified 1D framework can reproduce not only thermal and cure evolution but also process resistance trends over a range of pulling speeds.

Parametric analysis with the mathematical model quantifies the tradeoff between productivity and cure completeness, showing that increasing pulling speed reduces die-exit DoC and shifts gelation and peak force downstream, while lower speeds provide diminishing gains in cure. Within the current heater configuration, pulling speeds up to approximately 50–55 $cm \cdot min^{-1}$ achieve a practical in-die DoC target of 95% without excessive pulling resistance. Overall, the validated 1D model offers a computationally efficient tool for process window exploration and pulling force prediction, while the 3D ANSYS framework provides a complementary higher fidelity benchmark that can be extended toward coupled thermo–chemo–mechanical simulations of modulus, stress, and defect evolution in future work.

Acknowledgement

The research is funded within the Department of Energy DE-EE0011184 Project entitled “Pultrusion of structural components made of lignin-based carbon fiber”. We would also like to acknowledge BASF Inc. North America for providing polyurethane resin. Special thanks to Dr. Ali Zolali and Dr. Elias Shakour. PulFlex Techonologies, LLC provided pultrusion lines.

References

[1] AM Fairuz, SM Sapuan, ES Zainudin, and CNA Jaafar. Polymer composite manufacturing using a pultrusion process: A review. American Journal of Applied Sciences, 11(10):1798, 2014.

[2] Nik Poppe, Michael Wilhelm, and Luise Karger. Pultrusion process simulation-modelling of the injection and impregnation chamber. In Proceedings of the 2023 International Conference on Composite Materials, 2023.

[3] Pierpaolo Carlone, Ismet Baran, Jesper Henri Hattel, and Gaetano Salvatore Palazzo. Computational approaches for modeling the multiphysics in pultrusion process. Advances in Mechanical Engineering, 5:301875, 2013.

[4] Segun Isaac Talabi, Jim Tobin, Benjamin Strom, Ian Brownstein, Vlastimil Kunc, and Ahmed Arabi Hassen. Recent and future developments in pultrusion technology with consideration for curved geometries: A review. Composites Part B: Engineering, 283:111678, 2024.

[5] Costa Dias, R.C. Pultrusion of thermoset-based profiles – state of the art regarding materials, process set-ups, process modeling, and process simulation. Doctoral Thesis, Montanuniversität Leoben, Leoben, Austria, February 2020.

[6] Evgeny Barkanov, Pavel Akishin, Nora L Miazza, and Santiago Galvez. Ansys-based algorithms for a simulation of pultrusion processes. Mechanics of Advanced Materials and Structures, 24(5):377–384, 2017.

[7] Adam Douglas Freed. Modeling the pultrusion process to obtain low void fraction composites. West Virginia University, 2002.

[8] P Akishin, E Barkanov, and A Bondarchuk. Finite element modelling and analysis of conventional pultrusion processes. In IOP Conference Series: Materials Science and Engineering, volume 96, page 012012. IOP Publishing, 2015.

[9] G Ganesan and G Kumaran. An experimental study on the behaviour of gfrp pultruded i beam reinforced with cfrp laminates. International Journal of Advanced Technology and Engineering Exploration, 5(45):232–242, 2018.

[10] Xiao Lin Liu, IG Crouch, and YC Lam. Simulation of heat transfer and cure in pultrusion with a general-purpose finite element package. Composites Science and Technology, 60(6):857–864, 2000.

[11] Xueliang Ding, Quanguo He, Qun Yang, Suwei Wang, and Ke Chen. Numerical simulation of impregnation process of reactive injection pultrusion for glass fiber/pa6 composites. Polymers, 14(4):666, 2022.

[12] Arindam Mukherji and James Njuguna. An assessment on effect of process parameters on pull force during pultrusion. The International Journal of Advanced Manufacturing Technology, 121(5):3419–3438, 2022.

[13] Gibson Leonard Batch. Crosslinking free radical kinetics and the pultrusion processing of composites. University of Minnesota, 1989.

[14] Alexander A Safonov, Pierpaolo Carlone, and Iskander Akhatov. Mathematical simulation of pultrusion processes: A review. Composite Structures, 184:153–177, 2018.

[15] Claudia Garschke, Patricia P Parlevliet, Christian Weimer, and Bronwyn Louise Fox. Cure kinetics and viscosity modelling of a high-performance epoxy resin film. Polymer Testing, 32(1):150–157, 2013.

[16] Ismet Baran, Remko Akkerman, and Jesper H Hattel. Material characterization of a polyester resin system for the pultrusion process. Composites Part B: Engineering, 64:194–201, 2014.

[17] RP Theriault, TA Osswald, and JM Castro. A numerical model of the viscosity of an epoxy prepreg resin system. Polymer composites, 20(5):628–633, 1999.

[18] San Michael Sandberg, Onur Yuksel, Raphael Benjamin Comminal, Mads Rostgaard Sonne, Masoud Jabbari, Martin Larsen, Filip Bo Salling, Ismet Baran, Jon Spangenberg, and Jesper H Hattel. Numerical modeling of the mechanics of pultrusion. In Mechanics of materials in modern manufacturing methods and processing techniques, pages 173–195. Elsevier, 2020.

[19] Ranjeetkumar Gupta, Daniel Mitchell, Jamie Blanche, Sam Harper, Wenshuo Tang, Ketan Pancholi, Lee Baines, David G Bucknall, and David Flynn. A review of sensing technologies for non-destructive evaluation of structural composite materials. Journal of Composites Science, 5(12):319, 2021.

[20] Helena Rocha, Christopher Semprimoschnig, and João P Nunes. Sensors for process and structural health monitoring of aerospace composites: A review. Engineering Structures, 237:112231, 2021.

[21] Omogbai Oleghe. A predictive noise correction methodology for manufacturing process datasets. Journal of Big Data, 7(1):89, 2020.

[22] Wilma Polini and Andrea Corrado. Digital twin of composite assembly manufacturing process. International Journal of Production Research, 58(17):5238–5252, 2020.